New, High-Performance, Hydrogenated Paramagnetic Solution for Use in Earth Field DNP-NMR Magnetometers

K. Lang,[†,‡] M. Moussavi,[‡] and E. Belorizky*[,§]

Société ARPE, 72 avenue des Martyrs, 38000 Grenoble, France, LETI/DMEL Technologies Avancées-CEA/ Grenoble 17 rue des Martyrs, 38054 Grenoble Cédex 9, France, and Laboratoire de Spectrométrie Physique (CNRS-UMR 5588), Université Joseph Fourier/Grenoble 1, BP 87, 38402 Saint Martin d'Hères Cédex, France

Received: July 29, 1996; In Final Form: November 19, 1996[⊗]

The low-field nuclear magnetic resonance signals of solvent protons, enhanced by dynamic polarization, have been measured using a new paramagnetic solution of 1,1,3,3-tetramethylisoindol-*N*-oxyl (TMIO) free radical in triethylene glycol dimethyl ether (triglyme). The signal characteristics are compared with those of our previous standard solution for Earth field magnetometers. Enhancement factors varying between 1000 and 2000 are obtained between 25 and 125 °C; these results, which are the best ever obtained for stable radicals over such a large temperature range, are interpreted in the framework of relaxation matrix formalism with the help of extensive EPR line width measurements. In addition, this system is very efficient in high magnetic field gradients, owing to the relatively short NMR relaxation times T_2.

I. Introduction

Dynamic nuclear polarization (DNP) by paramagnetic impurities (Abragam Overhauser effect[1]) is a very efficient method for amplifying a NMR signal in low fields. In a solution this amplification is obtained through the magnetic coupling between the solvent protons and the free electrons of the paramagnetic molecules after saturation of the electronic transitions. This effect is the basic principle underlying high sensitivity magnetometers. The DNP enhancement factor is strongly dependent on the nature of the paramagnetic solution. A review of the various investigated systems was given by Müller Warmuth and Meise-Gresch.[2] It is known that the enhancement factor is considerably increased when the paramagnetic impurities have a strong hyperfine structure. For this reason it is convenient to use free radicals with a hyperfine coupling between the free electron and a nucleus of the same radical. The first system used for this purpose was the Fremy salt $NO(SO_3)_2^{2-}$ in water.[3−6] This radical, which becomes unstable after few days, was followed by a second generation of much more stable radicals based on cyclic carbon chains such as Tempol,[6] Tempone,[7,8] Tanane with a six or five carbon cyclic chain.[8,9] These different radicals were studied in various solvents such as methanol, benzene, and acetone or mixed hydrogenated and fluorinated solvents.[10−12] For magnetometry purposes Tempone free radicals in methanol are the most extensively used system. Hydrogenated and deuterated radicals were used with both ^{15}N and ^{14}N isotopes leading to two and three EPR transitions, respectively.[13,14] This system is stable at room temperature but has a lifetime of only about 150 h at 150 °C. The DNP enhancement factor[15] is about 1200 at 20 °C. Besides the above nitroxide radicals, phosphoniumyl free radicals were also synthesized.[16−18] The advantage of using phosphorus instead of nitrogen results from hyperfine coupling with the free electron radical that is 1 order of magnitude higher ($A \approx 700$ MHz) than for nitroxide radicals (60 MHz). So one could expect much higher DNP enhancement factors. Unfortunately these radicals are very unstable and the EPR lines are very broad.

Several scalar earth field DNP-NMR magnetometers have been built in our laboratory.[19,20] They are based on 2,2,5,5-tetramethylpyrrolidin-1-oxyl, Tanane, free radicals with various solvents according to the needs of the application: antisubmarine warfare, geological surveys, or bore hole logging. The DNP-NMR magnetometer is an excellent probe for oil prospecting as it provides very detailed information on rock magnetism. But in the deepest bore holes, ambient temperature is very high and may exceed 150 °C. The presence of magnetic muds also generates large magnetic field gradients. These two factors prevent the magnetometer from working properly. In this paper, a new paramagnetic solution that is efficient in rather high magnetic field gradients in a wide range of temperatures and which remains stable at high temperature is presented. This solution is a distilled triglyme, (triethylene glycol dimethyl ether) containing paramagnetic free radicals called TMIO (1,1,3,3-tetramethylisoindol-*N*-oxyl).[21] This solution, further denoted Ia and Ib for radical concentrations 10^{-3} mol L^{-1} and 2×10^{-3} mol L^{-1} respectively, can expand significantly the range of use of the magnetometer. Its characteristics are compared to those of water mixed with a 5% diglyme (diethylene glycol dimethyl ether) solution with 10^{-3} mol L^{-1} of Tanane free radical.[8,22] The latter was our previous best reference solution and is denoted as solution II. In section 2, we sketch the theoretical expression for the DNP enhancement factor and for the EPR line width. The experimental procedure is given in section 3. The measured temperature variation of the DNP factor for our three solutions is given in section 4 and compared with the theoretical predictions. In section 5, the behavior of the enhanced resonance signals, in presence of external magnetic field gradients, is investigated. The respective performances of our solutions are then related to the transverse nuclear relaxation times in low fields.

II. NMR Signal Enhancement Factor with DNP

Theory. In weak magnetic fields, nuclear magnetism is hardly detectable. At thermodynamic equilibrium, the Boltzmann distribution leads to the nuclear spin polarization[23] $P_0 = \langle I_z \rangle / I = I_0 / I$, which for spin $I = {}^1/_2$ is given by $P_0 = \hbar\omega_I / 2kT$, where ω_I is the nuclear resonance angular frequency. The

* Author to whom all correspondence should be addressed.
† Société ARPE.
‡ LETI/DMEL Technologies Avancées.
§ Université Joseph Fourier.
⊗ Abstract published in *Advance ACS Abstracts,* February 1, 1997.

S1089-5639(96)02283-9 CCC: $14.00

macroscopic nuclear magnetization is then $M_0 = N_I\gamma_I\hbar IP_0$, where N_I is the number density of nuclei with gyromagnetic factor γ_I.

To amplify the detected signal, a significant enhancement of the polarization is required. This is achieved by coupling the nuclear spin system to an electronic spin system of free radicals, which are added to the solvent. The coupling between both systems arises from magnetic dipolar interaction or (and) hyperfine scalar interactions.[2,24] The relative magnitude of these interactions depends on the nature of the resonant nuclei and of the solvent and radical molecules. Owing to cross-relaxation transitions, the polarization becomes:[4]

$$P = P_0 - \rho f(\langle S_z\rangle - S_0)/I \tag{1}$$

where $\langle S_z\rangle$ and S_0 are the electronic polarization and its corresponding value at thermal equilibrium respectively. In the above equation, ρ is characteristic of the coupling mechanism between the electronic spin S and the nuclear spin I ($\rho = 0.5$ for pure dipolar interaction and $\rho = -1$ for pure scalar hyperfine coupling) and f is the coupling efficiency factor with $f = 1$ in the ideal case where the nuclear spins would only relax through their coupling with the spins S. In general we have $0 < f < 1$. If the electronic transition is saturated $\langle S_z\rangle = 0$, and the enhancement factor F is

$$F = \frac{P}{P_0} = 1 + \rho f\frac{S_0}{I_0} \approx \rho f\frac{S_0}{I_0} \tag{2}$$

For electronic spins $S = {}^1/_2$, $S_0 = \hbar\omega_S/2kT$, where ω_S is the electronic angular frequency and in the case of a pure dipolar coupling with the protons of the solution

$$F = \frac{1}{2}f\frac{S_0}{I_0} = -\frac{1}{2}f\frac{\gamma_S}{\gamma_I} = -330 \tag{3}$$

A much larger dynamic polarization factor F may be obtained when the electronic spin S of the free radical is coupled through an hyperfine scalar interaction $\mathbf{H} = \hbar A\vec{S}\cdot\vec{K}$ with a nuclear spin K belonging to the radical.[8,11] Then, after saturation of a selected electronic transition, the presence of a local hyperfine magnetic field, much larger than the Earth's magnetic field, leads to a value of $\langle S_z\rangle$ much larger than S_0, and according to eqs 1 and 2, F is of the order of $-\rho f\langle S_z\rangle/I_0$. More precisely if $K = {}^1/_2$ like for ^{15}N nucleus in our free radicals, the level scheme of the radical under an external magnetic field H_0 is shown in Figure 1.

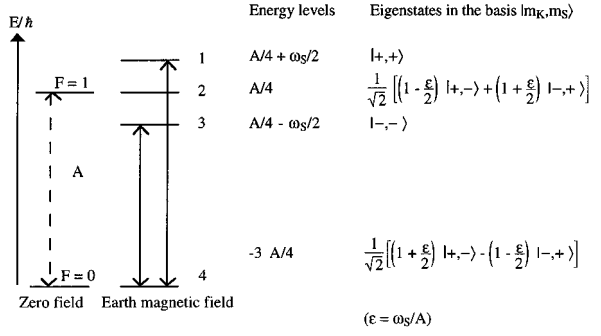

Figure 1. Energy levels and associated eigenstates of our free radicals with an isotropic hyperfine coupling A $\vec{S}\cdot\vec{K}$ between the free electron $S = {}^1/_2$ and the ^{15}N nucleus $K = {}^1/_2$ under an external weak magnetic field. The arrows indicate the relevant allowed electronic transitions $1 \leftrightarrow 4$ and $3 \leftrightarrow 4$. In zero field if $\vec{F} = \vec{K} + \vec{S}$, F is a good quantum number.

There are four levels denoted 1−4 and two electronic transitions $1 \leftrightarrow 4$ and $3 \leftrightarrow 4$ with angular frequencies $\omega_{14} = A + \omega_S/2$ and $\omega_{34} = A - \omega_S/2$ close to A. In a first step neglecting any relaxation phenomenon, the theoretical DNP factors after saturation of the $1 \leftrightarrow 4$ or $3 \leftrightarrow 4$ transition, for a purely dipolar coupling with the solvent protons, are[10]

$$F_{14} = -\frac{1}{8}\frac{A}{\omega_I}\left(1 + \frac{3}{2}\frac{\omega_S}{A}\right)f \quad \text{and} \quad F_{34} = -\frac{1}{8}\frac{A}{\omega_I}\left(1 - \frac{3}{2}\frac{\omega_S}{A}\right)f \tag{4}$$

The above factors are lowered by the electronic relaxation through four main mechanisms:

(i) the spin rotational interaction $\mathbf{H}_{SR}(t) = \hbar\,\vec{S}\cdot\bar{\bar{C}}\cdot\vec{J}$ where $\bar{\bar{C}}$ is the spin rotational tensor and $\vec{J}$ the rotational angular momentum of the molecule,[13]

(ii) the anisotropic part of the hyperfine coupling[25] $\mathbf{H}_{HF}(t) = \hbar\,\vec{S}\cdot\bar{\bar{A}}\cdot\vec{K}$ with the nuclear spin K of the radical, where $\bar{\bar{A}}$ is the hyperfine tensor,

(iii) the magnetic dipolar coupling $\mathbf{H}_{DIP}(t)$ between two free radicals with spins $\vec{S}_1$ and $\vec{S}_2$, and

(iv) the exchange interaction[26] between $\vec{S}_1$ and $\vec{S}_2$, $\mathbf{H}_{EX}(t) = hJ\,\vec{S}_1\cdot\vec{S}_2$.

Mechanisms i and ii are intramolecular (within the radical), while iii and iv are intermolecular (between different radicals). The relative importance of these effects can be estimated only through line width studies in high magnetic fields. Finally, according to eq 1, for a pure dipolar coupling of the protons with the free radicals the dynamic polarization factor is

$$F = \frac{P}{P_0} = -\frac{f}{2I_0}(\langle S_z\rangle - S_0) \tag{5}$$

which can be rewritten[14,27] as

$$F = -\frac{fA}{2\omega_I}\Phi(\omega_S,\omega_1,\omega,A,\Delta H) \tag{6}$$

Φ is a complicated function involving the isotropic hyperfine constant A, $\omega_S = |\gamma_S|H_0$, $\omega_1 = |\gamma_S|H_1$, H_0 and H_1 being the Earth's magnetic field and the radiofrequency field rotating at angular frequency ω; ΔH is the EPR line width of the $1 \leftrightarrow 4$ transition. The derivation of the function Φ is given in the Appendix. Here we outline the fact that ΔH is an essential ingredient of the problem. Quite generally F is a decreasing function of ΔH which means that narrow lines are required for high signal enhancements. Unfortunately, ΔH can be measured only in high magnetic fields through EPR measurement, but it is easy to derive the values of ΔH in low fields involved in eq 6 from the experimental high-field values. These determinations result from general relaxation theory; the approximations that are made concern the independence of the various relaxation processes and the assumption that all the correlation times are short enough to replace the various spectral densities $J(\omega)$ by their extreme narrowing limit $J(0)$, a condition which is easily satisfied at low fields for these rather low-viscosity solutions. Consequently no appreciable error is expected for this extrapolation. The influence of the EPR line width is discussed in the following subsection.

EPR Line Widths. The EPR experiments were performed in the X band (9 GHz). The broadening of the lines arises from the four relaxation mechanisms previously quoted. Assuming Lorentzian line shapes, the EPR line width ΔH^X defined as the peak to peak distance of the derivative of the absorption curve is related to the transverse relaxation time T_2 by

$$\left(\frac{1}{T_2}\right)^X = \frac{\sqrt{3}\gamma_S}{2}\Delta H^X \tag{7}$$

where γ_S is the electronic spin gyromagnetic factor and ΔH^X is given by

$$\Delta H^X = \Delta H^X_{SR} + \Delta H^X_{HF} + \Delta H^X_{DIP} + \Delta H^X_{EX} + C_I \quad (8)$$

In the above expression, SR, HF correspond to the spin rotational and hyperfine couplings, respectively, while DIP and EX refer to dipolar and exchange interactions between different radicals. C_I is a constant contribution to the EPR line broadening due to the unresolved hyperfine structure with the protons of the radical molecule.[17] We now determine the theoretical expressions for the various contributions to $(1/T_2)^X$.

(i) Spin Rotational effect. For a paramagnetic molecule with axial symmetry, it was shown[28] that

$$\left(\frac{1}{T_2}\right)^X_{SR} = (\Delta g_{||}^2 + 2\Delta g_\perp^2)\frac{kT}{12\pi r_e^3 \eta} \quad (9)$$

where $\Delta g_i = g_i - 2.0023$ expresses the departure of the **g** tensor components from the free spin value, η is the solvent viscosity, and r_e is the effective radius of the paramagnetic molecule.[13]

(ii) Anisotropic Hyperfine Coupling Effect. Similarly it was shown[25] that for a paramagnetic molecule with axial symmetry and a nuclear spin K

$$\left(\frac{1}{T_2}\right)^X_{HF} = \tau_r\left[\frac{1}{40}(\Delta A)^2 + \frac{1}{45}(\Delta g \omega_S)^2 + \frac{4}{45}(\Delta A)(\Delta g)\omega_S m_K + \frac{1}{18}(\Delta A)^2 m_K^2\right] \quad (10)$$

where $\tau_r = (4\pi\eta r_e^3)/(3kT)$ is the rotational correlation time, $\Delta A = A_{||} - A_\perp$, $\Delta g = g_{||} - g_\perp$, and $m_K = \pm 1/2$ for a ^{15}N nucleus.

(iii) Magnetic Dipolar Coupling Effect. $(1/T_2)^X_{DIP}$ is proportional to N_S/Db, where N_S is the number of free radicals per unit volume, b is the minimum distance of approach of the centres of two diffusing radicals, and D is their relative diffusion constant; this contribution will be important at low temperatures when we have a viscous solution. Then $\omega_S\tau \gg 1$, τ being the translational correlation time $\tau = b^2/D$. Consequently in the well-known[23,29] expression for $1/T_2$ we have only a contribution from the spectral density of $r^{-3}Y_{2,0}(\theta,\varphi)$, where r, θ, φ refer to the relative position of the two interacting spins, i.e. of $J(0)$. Furthermore when both radicals have the same value of m_K, they can be considered as identical electronic spins, but when the respective values of m_K are different, we have a dipolar interaction between unlike electronic spins having slightly different gyromagnetic factors. For $K = 1/2$ we have the same proportion of like and unlike couples of spins. Then

$$\left(\frac{1}{T_2}\right)^X_{DIP} = \left(\frac{\mu_0}{4\pi}\right)^2 \frac{1}{2}\left[\frac{3}{5}\gamma_S^4 h^2 S(S+1)J(0) + \frac{1}{3}\gamma_S^4 h^2 S(S+1)J(0)\right]$$

where both contributions are separated. Neglecting pair correlation and eccentricity effects it was shown[30] that

$$J(0) = \frac{4}{27\pi}\frac{N_S}{Db} \quad (11)$$

Then, with $S = 1/2$, we obtain

$$\left(\frac{1}{T_2}\right)^X_{DIP} = \left(\frac{\mu_0}{4\pi}\right)^2 \frac{7}{135} h^2 \frac{N_S}{\pi D b}$$

Assuming that $D = (4kT)/(6\pi b^*\eta)$, where b^* is an effective distance which can significantly differ from b, we get

$$\left(\frac{1}{T_2}\right)^X_{DIP} = \left(\frac{\mu_0}{4\pi}\right)^2 \frac{7}{90}\frac{\gamma_S^4 h^2}{kT}\frac{b^*}{b}\eta N_S \quad (12)$$

(iv) Exchange Coupling Effect. This effect has been the subject of extensive studies. Ayant[26] developed a simple model in which the exchange integral J (expressed in frequency units) between two diffusing radicals with a different nuclear spin state m_K is zero for $r > r_0$ and has a constant value for $b < r < r_0$, where r is the interspin distance and r_0 the radius of an effective "collision" sphere. *I*t was shown that for $K = 1/2$

$$\left(\frac{1}{T_2}\right)^X_{EX} = \frac{2 r_0 kT}{3b^*\eta}\varphi(u) N_S \quad (13a)$$

where b^* has been defined above, $u = (1/r_0)(D/(2J))^{1/2}$ and $\varphi(u)$ is defined by

$$\varphi(u) = 1 - \mathrm{Re}\frac{\lambda + \frac{u}{\zeta}\tanh\left[(1-\lambda)\frac{\zeta}{u}\right]}{1 + \frac{\lambda\zeta}{u}\tanh\left[(1-\lambda)\frac{\zeta}{u}\right]} \quad (13b)$$

with $\zeta = (i/2)^{1/2}$ and $\lambda = b/r_0$. The function $\varphi(u)$ has been tabulated[26] for several values of λ ranging between 0.2 and 0.8. Finally, setting

$$x = \frac{T}{10^4\eta} \quad (14)$$

we have according to eqs 7−14

$$\Delta H^X(T) = \alpha_{SR}x + \frac{\alpha_{HF}}{x} + \left[\frac{\alpha_{DIP}}{x} + \alpha_{EX}x\varphi(P\sqrt{x})\right]c_S + C_I \quad (15)$$

where c_S is the free radical concentration in mol L^{-1}, and in SI units

$$\alpha_{SR} = \frac{2.4 \times 10^{-32}}{r_e^3}(\Delta g_{||}^2 + 2\Delta g_\perp^2) \quad (16a)$$

$$\alpha_{HF} = 2 \times 10^8 r_e^3\left[\frac{1}{40}(\Delta A)^2 + \frac{1}{45}(\Delta g \omega_S)^2 + \frac{4}{45}(\Delta A)(\Delta g)\omega_S m_K + \frac{1}{18}(\Delta A)^2 m_K^2\right] \quad (16b)$$

$$\alpha_{DIP} = 9.4 \times 10^{-3}\frac{b^*}{b} \quad (16c)$$

$$\alpha_{EX} = 36.35 \times 10^{-5}\frac{r_0}{b^*} \quad (16d)$$

$$P = 1.2 \times 10^{-9}(r_0^2 b^* J)^{-1/2} \quad (16e)$$

III. Experimental Section

Sample Preparation. Tanane (2,2,5,5-tetramethylpyrrolidin-1-oxyl-$^{15}N,d_{16}$) was purchased from Eurisotope (Orsay, France). TMIO (1,1,3,3-tetramethylisoindol-*N*-oxyl-$^{15}N,d_{12}$) was synthesized by Dr. Xiao Ping Wu at the Department of Chemistry, University of Surrey (Guildford, U.K.).[21] Diethylene glycol dimethyl ether (diglyme) was purchased from Aldrich and used without any further purification. Triethylene glycol dimethyl

ether also provided by Aldrich was distilled twice at low pressure (120 °C, 50 Torr) over NaH. All solutions (Tanane 10^{-3} mol L^{-1} in water mixed with 5% diglyme and TMIO 10^{-3} and 2×10^{-3} mol L^{-1} in triglyme) were degassed in appropriate flasks and then vacuum sealed.

NMR and EPR Experiments. DNP-NMR measurements were performed on a homemade double-resonance spectrometer[31] working between 1950 and 2000 Hz for the nuclear frequency and between 40 and 300 MHz for the electronic frequency. All measurements were performed in the ambient Earth's magnetic field in the mountains near Grenoble, where human magnetic disturbances are weak. The sensor is located in a special amagnetic heat-regulated room (where the applied temperature may be varied from −50 up to 180 °C). The probe is made of a cell containing the paramagnetic solution. This cell is also a HF resonator in order to induce the electronic resonance. The low-frequency circuit consists of two orthogonal coils in order to induce and detect the nuclear resonance.

For nuclear relaxation time measurements, we used a homemade relaxometer consisting of two symmetrical coils perpendicular to the Earth's magnetic field H_0. One coil contains the flask with the diamagnetic or paramagnetic solution; the other is empty. First a rather strong magnetic field H_p ($H_p \approx 10^{-2}$ T) is created by the coils, whose effect is to polarize the solution and to create a transverse magnetization M_p. Then this polarization field is removed, and one measures the temporal attenuation of the free precession magnetic signal M_t in the Earth's magnetic field. In fact the signal is recorded through a differential amplifier connected to the two coils in order to eliminate the external perturbations of the local Earth's magnetic field variations and the eddy currents which are present just after the polarization field cutoff. We have

$$M_t = M_p \exp(-t/T_2^*) \tag{17}$$

where T_2^* includes contributions from field inhomogeneities.

Several experiments with different values of the polarization times t_p of the solution provide the longitudinal relaxation time T_1 through the relation

$$M_p = M_{p0}[1 - \exp(-t_p/T_1)] \tag{18}$$

with an appropriate fitting procedure.

With this simple technique T_1 is given with a good accuracy (less than 10%), but we are not able to extract a value of T_2 from the measured value of T_2^* as the spin−echo technique is not available in this frequency range.

High-field EPR experiments were performed on a Bruker 9 GHz spectrometer.

IV. Applications to our Solutions

EPR in High Fields. The various parameters involved for the reference solution II were given previously[32,33] and will be simply recalled for comparison with our new solutions Ia and Ib whose properties are detailed below. EPR measurements[21] in solid solutions of TMIO in toluene gave $g_x = 2.0015$, $g_y = 2.0052$, and $g_z = 2.0082$. We take $g_{\parallel} = g_x$ and $g_{\perp} = (g_y + g_z)/2 = 2.0067$. Then from eq 16a $\alpha_{SR} = 10^{-36}/r_e^3$. The hyperfine structure with the ^{14}N isotope was also observed[21] and led to $A_{xx} = 5.95 \times 10^8$ rd s^{-1} (3.38×10^{-3} T), $A_{yy} = 7.73 \times 10^7$ rd s^{-1} (4.39×10^{-4} T), $A_{zz} = 8.8 \times 10^7$ rd s^{-1} (5×10^{-4} T). Then the isotropic hyperfine constant is $A = (A_{xx} + A_{yy} + A_{zz})/3 = 2.53 \times 10^8$ rd s^{-1} (1.44×10^{-3} T).

The anisotropy of the hyperfine coupling is taken as $\Delta A = A_{xx} - (A_{yy} + A_{zz})/2 = 5.12 \times 10^8$ rd s^{-1} (2.91×10^{-3} T). The hyperfine coupling is proportional to the nuclear gyromagnetic factor[34] and since $\gamma^{15}N/\gamma^{14}N = 1.4$, we take for TMIO with the ^{15}N isotope $A = 3.54 \times 10^8$ rd s^{-1} (2.01×10^{-3} T). This value is in agreement with our measured value of the splitting between the two EPR lines at 280 MHz in our liquid solution. These lines correspond to the transitions $^1/_2$, $m_K \leftrightarrow -^1/_2$, m_K with $m_K = \pm^1/_2$ and energies $\omega_S \pm A/2$. Note that the same value of A is obtained from the low-field spectrum by taking the average energy between the transitions $1 \leftrightarrow 4$ and $3 \leftrightarrow 4$ (Figure 1). Then from eq 16b, taking $\Delta A = 7.17 \times 10^7$ rd s^{-1}, $\alpha_{HF} = 2.5 \times 10^{24} r_e^3$ or $6.3 \times 10^{24} r_e^3$ for $m_K = \pm^1/_2$, respectively.

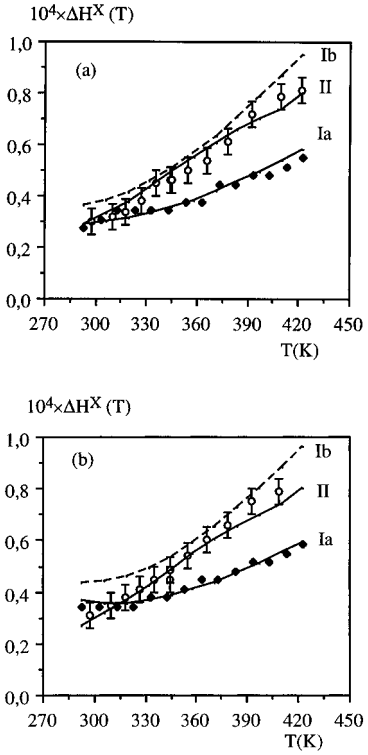

Figure 2. Temperature dependence of the EPR line widths in high fields of solutions Ia, Ib, and II: (a) transition $1 \leftrightarrow 4$, (b) $3 \leftrightarrow 4$. For solutions Ia and II the continuous curves are the results of a least-squares fit of the unknown parameters (see text and Table 1). For solution Ib the dashed curve is calculated using the parameters obtained for solution Ia.

The above values are inserted into eq 15. The minimum distance of approach between the centers of the TMIO and triglyme molecules, considered as hard spheres, was determined, first using the CPK compact model and second using the theoretical Connoly method.[35] Both methods gave $b = 7.3 \times 10^{-10}$ m. Then, according to eqs 15 and 16, the unknown parameters are r_e, J, C_I, and the ratios b^*/b and r_0/b^*.

In Figure 2 we display the measured temperature dependence of the EPR line width of the transitions $1 \leftrightarrow 4$ and $3 \leftrightarrow 4$ for two concentrations of our solution, $c_S = 10^{-3}$ mol L^{-1} (solution Ia) and $c_S = 2 \times 10^{-3}$ mol L^{-1} (solution Ib) and for the reference solution II. In this figure we also show the calculated values of ΔH^X obtained by a least-squares fit of the unknown parameters listed in Table 1. Good agreement is obtained between the measured and calculated values of ΔH^X. The most striking feature displayed by Figure 2 is that the EPR line width of solution Ia is about half that of reference solution II, varying between 0.27×10^{-4} and 0.55×10^{-4} T between $T = 293$ and 423 K. These are remarkably low values. It is seen that solution Ib provides EPR linewidths comparable to those of the reference.

It is interesting to separate the contributions of the various mechanisms to the total EPR line width. With the parameters given in Table 1, we determine the various α defined by eqs 16 for solutions Ia and II (see Table 2). Using the experimental

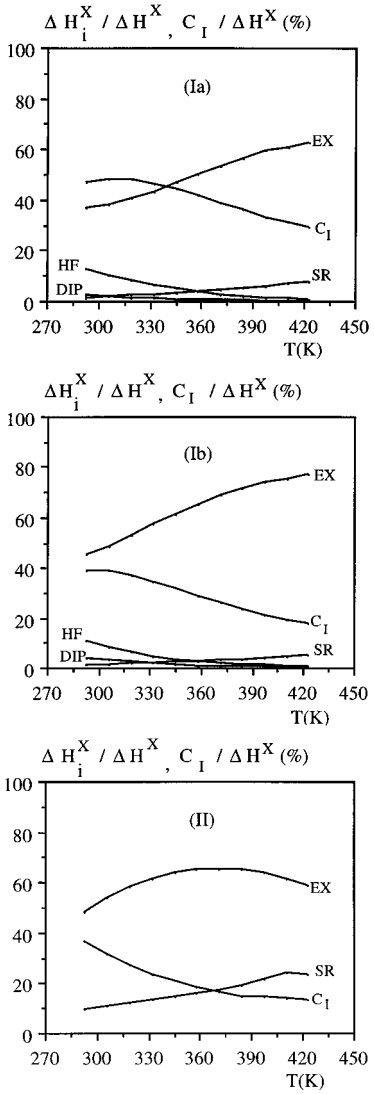

Figure 3. Relative contribution of the various broadening mechanisms of the high-field line width versus temperature for solutions Ia, Ib, and II. Contributions of ΔH^X_{DIP} and ΔH^X_{HF} are negligible for solution II.

TABLE 1: Physical Constants of the Model

solution	TMIO + triglyme (solutions Ia and Ib)	Tanane + water + 5% diglyme (solution II)
$g_{\|\|}$	2.0015	2.0022
$g_\perp$	2.0067	2.0077
ΔA (10^{-4} T)	40.7	36.4
b (m)	7.2×10^{-10}	4.8×10^{-10}
r_e (m)	3×10^{-10}	2.5×10^{-10}
b^*/b	1.3	1.5
r_0/b^*	1.3	1.5
J (s^{-1})	2×10^{10}	1.5×10^{10}
C_I (10^{-4} T)	0.17	0.1

TABLE 2: α and η Parameters in our Solutions (SI Units)

solution	TMIO + triglyme (solutions Ia and Ib)	Tanane + water + 5% diglyme (solution II)
$10^{11} \times \alpha_{SR}$	3.52×10^{-3}	8.9×10^{-3}
$10^{-3} \times \alpha_{HF}$	0.17 ($m_K = -1/2$)	0.085 ($m_K = -1/2$)
	0.067 ($m_K = 1/2$)	0.028 ($m_K = 1/2$)
$10^3 \times \alpha_{DIP}$	12.17	14
$10^5 \times \alpha_{EX}$	47.25	54.5
P	2.34×10^{-4}	3.06×10^{-4}
η (SI)	$1.165 \times 10^{-5} \exp(1517.7/T)$	$3.862 \times 10^{-6} \exp(1635.7/T)$

variation of the viscosity versus temperature, which can be easily described by the empirical laws given in Table 2, from eq 15 we calculate, $\Delta H_i^X/\Delta H^X$ and $C_I/\Delta H^X$ where i denotes each of the four relaxation processes. The results are displayed in Figure 3 in the temperature range 293 K < T < 423 K. It can be seen that in all solutions the exchange and spin rotational mechanisms are dominant and that the unresolved hyperfine structure with the protons of the radical molecule is always strong. But througout the investigated temperature range the dipolar and hyperfine relaxation mechanisms contribute negligibly in those low-concentration free radical solutions.

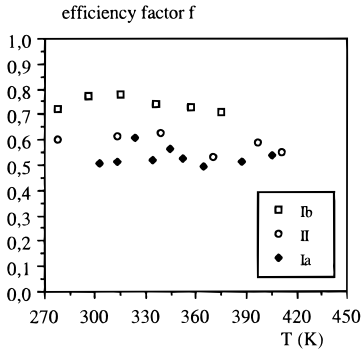

Figure 4. Experimental variation of the efficiency factor versus temperature for solutions Ia, Ib, and II.

Relaxation Matrix Elements and DNP Enhancement Factor. We introduce a relaxation matrix **R** that describes the time evolution of the populations of levels i due to the relaxation processes. More precisely, defining $x_i = (N_i - N_{i0})/N$ as the difference of the relative populations of level i from its value at thermal equilibrium, we have

$$\frac{dx_i}{dt} = -R_{ii}\, x_i + \sum_{j \neq i} R_{ij} x_j \tag{19}$$

It is shown in the Appendix that these relaxation matrix elements can be expressed in terms of four constants a, b, c, and d characteristic of each relaxation process and defined by eq A27. From eqs 7, 15, and A27 we obtain for various temperatures the values a, c, and d of the relaxation matrix given in Table 3. For the value of b, it was shown that in low fields[14]

$$\left(\frac{1}{T_2}\right)_{HF} = \frac{1}{18}(\Delta A)^2\, \tau_r \tag{20}$$

where ΔA is given in Table 1 and τ_r is easily calculated.

The corresponding values of $1/T_2$ in low fields given by eq A30 are also listed in Table 3 together with the calculated low-field EPR line width ΔH. Note that ΔH for solution Ia remains much lower than that of solutions Ib and II.

To calculate the DNP enhancement factor from eq A20 we have all the ingredients except the coupling efficiency factor f, which is given by

$$f = 1 - \frac{T_1}{T_{10}} \tag{21}$$

where T_{10} and T_1 are the longitudinal NMR relaxation times of the solvent protons in the diamagnetic and paramagnetic solutions respectively. The temperature behavior of this factor was determined experimentally in the Earth's magnetic field for all our solutions, and the results are displayed in Figure 4. It can be seen that f remains approximately constant with temperature and ranges between 0.5 and 0.7 for solutions Ia and Ib and is about 0.6 for solution II. As will be seen below the loss in the DNP factor of solution Ia due to the slightly lower value of f with respect to both other solutions is largely compensated by its much narrower EPR line width. The experimental NMR signals, enhanced by the effect of dynamic polarization, are displayed in Figure 5 for the three solutions at

TABLE 3: Relaxation Matrix Elements and EPR Line Widths of our Solutions in the Earth's Magnetic Field

	$T = 293$ K			$T = 345$ K			$T = 398$ K		
solution	Ia	Ib	II	Ia	Ib	II	Ia	Ib	II
a (s^{-1})	18988	18988	97313	48820	48820	265862	101190	101190	576761
b (s^{-1})	991584	991584	227528	385675	385675	83281	186070	186070	38389
c (s^{-1})	51811	103622	29635	20152	40304	10847	9722	19444	5000
d (s^{-1})	347947	695894	747377	857358	1.7×10^6	1.76×10^6	1.66×10^6	3.3×10^6	2.53×10^6
$1/T_2$ (s^{-1})	2.7×10^6	3.7×10^6	2.3×10^6	2.6×10^6	4.4×10^6	4.5×10^6	4.0×10^6	7.4×10^6	6.88×10^6
ΔH (10^{-4} T)	0.17	0.24	0.15	0.17	0.29	0.29	0.26	0.48	0.45

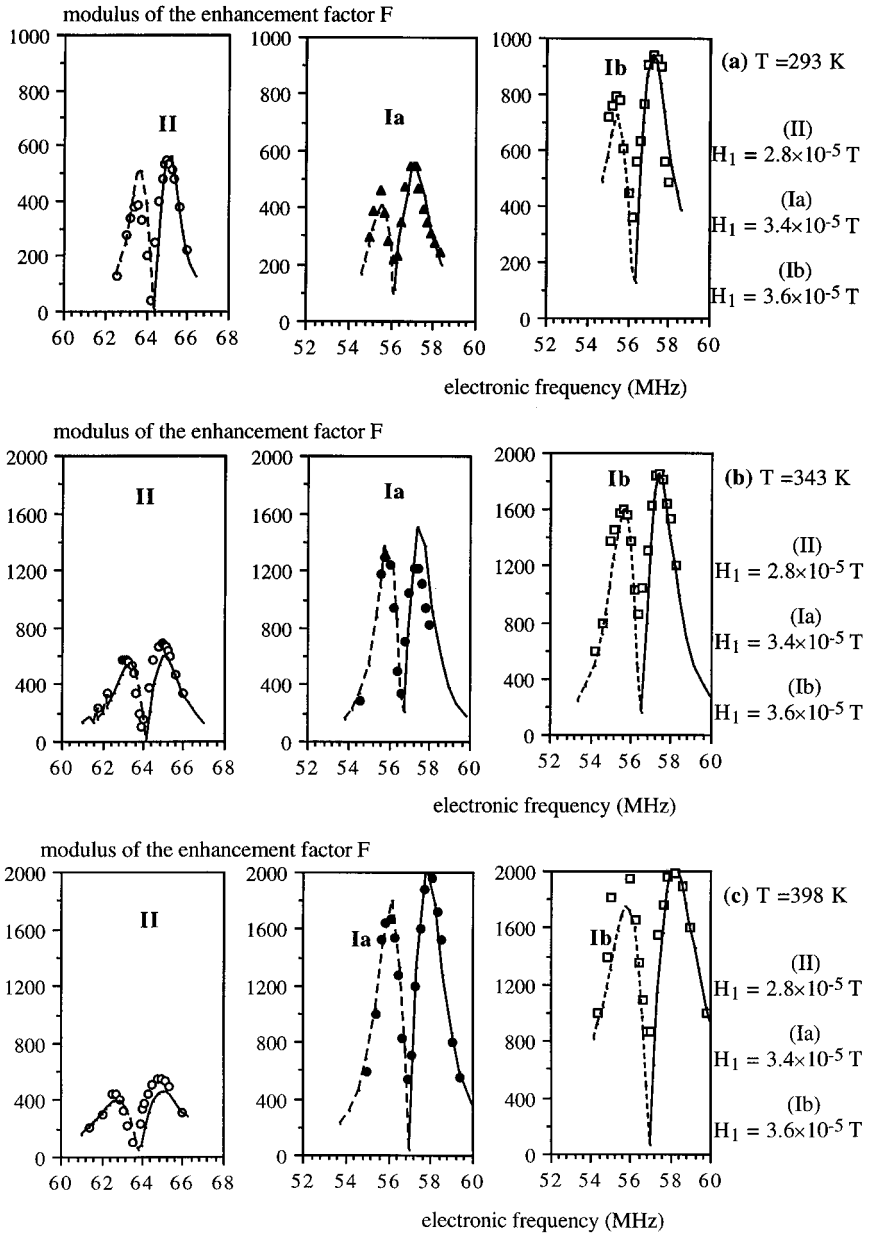

Figure 5. Frequency dependence of the DNP enhancement factor F for our solutions (a) $T = 293$ K, (b) $T = 343$ K, and (c) $T = 398$ K. Continuous and dotted curves indicate the theoretical values for the $1 \leftrightarrow 4$ and $3 \leftrightarrow 4$ transitions respectively. The values of H_1 giving the maximum DNP factor are given beside each figure.

different temperatures. The DNP factor F was calculated for various electronic frequencies ω in the range $A - \omega_S < \omega < A + \omega_S$. In each experiment the rotating field H_1 was chosen in such a way as to provide the highest F factor for the $1 \leftrightarrow 4$ transition. In the calculation of F we took into account the fact that in our cylindrical cavity H_1 is strongly inhomogeneous, both in magnitude and direction, and an average value was determined. The theoretical curves $F(\omega)$ were compared with the experimental spectra by attributing to the maximum amplitude of the $1 \leftrightarrow 4$ transition the calculated value of $F(A+\omega_S/2)$. The resulting calculated curves $F(\omega)$ are shown in Figure 5. We obtain remarkable agreement with the observed signals. It is clear that solution Ib provides the best F factor at all temperatures. The maximal value of F varies from 936 to 2056 from $T = 293-398$ K and reaches a maximum of 2086 for $T = 373$ K. No other stable solution provides comparable factors on such a wide temperature range.

V. NMR Signals in the Presence of Magnetic Field Gradients

NMR Signals. We have studied the effect of external magnetic gradients on the NMR signal of our solution. The

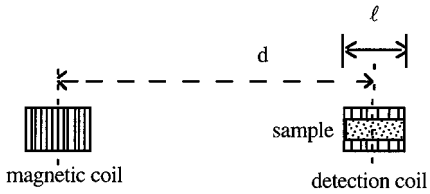

Figure 6. Schematic experimental disposal for inducing external magnetic field gradients.

magnetometer must keep its efficiency in the presence of magnetic muds. These generate strong field gradients that can reach values up to 10^{-6} T m^{-1}.

The samples containing 160 mL of solutions Ib and II were submitted to a constant gradient value of up to 10^{-6} T m^{-1}. This gradient field was created on the symmetry axis of a cylindrical magnetic coil at a large distance (about 1 m) from it. The amplitude of the DNP enhanced signal was measured for an EPR rf field H_1 rotating at a frequency ν_{14} corresponding to the maximum value of the DNP factor F for the $1 \leftrightarrow 4$ transition and for a nuclear excitation field H_{1n} rotating at an angular resonance frequency $\omega_0 = \gamma_I(H_0 + H)$, where H_0 is the Earth's magnetic field and H is the variable field created by the coil at the distance d. We denote by x the solvent proton position varying between $l/2$ and $-l/2$, l being the tube length in axial position around the mean distance d (see Figure 6). Under our experimental conditions we have $H(x) = H + gx$ with $g = -(3H)/d$, where g is the gradient field. In Figure 7 we display the variation of this amplitude for various gradient fields obtained by increasing the current in the coil at different temperatures. It is seen that in presence of external gradient fields, the attenuation of the signal amplitude of solution Ib is lower than that of solution II. Qualitatively this is explained by a shorter transverse relaxation time T_2 of solution Ib. More precisely, assuming a normalized Lorentzian line shape $f(\omega)$ of the NMR signal, we have

$$f(\omega) = \frac{\sigma}{\pi}\frac{1}{(\omega - \omega_0)^2 + \sigma^2} \tag{22}$$

$$\text{with} \quad \sigma = \frac{1}{T_2^*} = \frac{1}{T_2} + \frac{1}{T_2'} \tag{23}$$

where T_2 is the true transverse relaxation time and $T_2' = (\gamma\Delta H_0)^{-1}$, ΔH_0 being the field inhomogeneity in the recording coil, which is always present even in the absence of a superimposed external gradient field. The amplitude of the signal at the resonance frequency $\omega_0 = \gamma_I H_0$ is $f(\omega_0) = 1/\sigma\pi$. In presence of the external gradient field g, the Larmor resonance frequencies become $\omega(x) = \omega_0 + \omega'$ with $\omega' = \gamma_I g x$. ω' varies linearly between $\Delta\omega$ and $-\Delta\omega$ where $\Delta\omega = \gamma_I g l/2$, and the normalized distribution of ω' in this range is $h(\omega) = 1/(2\Delta\omega)$. The observed normalized resonance signal is then

$$f_g(\omega) = \frac{\sigma}{2\pi\Delta\omega}\int_{-\Delta\omega}^{\Delta\omega}\frac{d\omega'}{(\omega - \omega_0 - \omega')^2 + \sigma^2} = \frac{1}{2\pi\Delta\omega} \times \left[\arctan\left(\frac{\omega_0 - \omega + \Delta\omega}{\sigma}\right) - \arctan\left(\frac{\omega_0 - \omega - \Delta\omega}{\sigma}\right)\right] \tag{24}$$

The signal amplitude at the central resonance frequency $\omega = \omega_0$ becomes

$$f_g(\omega_0) = \frac{1}{\pi}\frac{\arctan(\Delta\omega/\sigma)}{\Delta\omega} \tag{25}$$

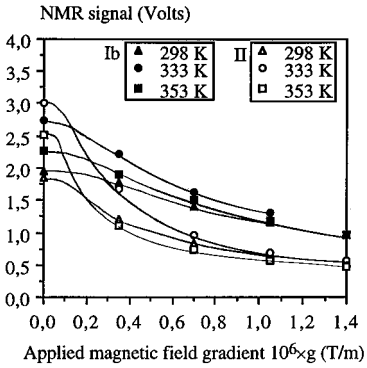

Figure 7. Effect of an external field gradient on the NMR signal of solutions Ib and II for various temperatures. For solution Ib and II, ν_{14} = 57.2 and 64.9 MHz respectively.

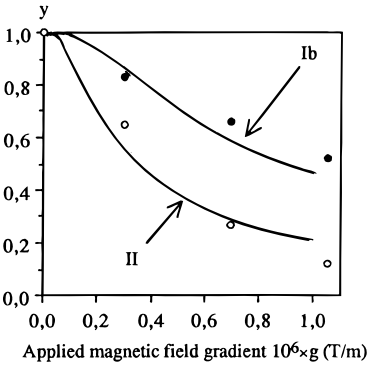

Figure 8. Attenuation of the amplitude of the enhanced NMR signals of solutions Ib and II of external magnetic field gradients. Continuous curves result from the theoretical expression 26 at 298 K and for l = 3.5 cm with the measured values T_2(Ib) = 0.55 s, T_2(II) = 1.4 s.

Then the ratio of the maximal amplitude signal in presence of external gradient with that without gradient is

$$y = \frac{f_g(\omega_0)}{f(\omega_0)} = \frac{\arctan(\Delta\omega/\sigma)}{\Delta\omega/\sigma} \tag{26}$$

It is clear that for a solution with a shorter transverse relaxation time T_2, σ will be larger and y will increase. Using the ratios of the measured values of T_2 for both solutions Ib and II at various temperatures, we have plotted in Figure 8 the theoretical variation of y which is compared with the experimental results. According to the experimental uncertainty on the T_2 values and of the rather crude theoretical model, the agreement is quite satisfactory. In conclusion solution Ib which exhibited the best dynamic polarization factor F is also much more efficient than solution II in the presence of magnetic field gradients.

Transverse Nuclear Relaxation Times in Low Fields. Now we explain why solution Ib has shorter transverse relaxation times than solution II. Neglecting any gradient field inhomogeneity, the transverse relaxation rate introduced in eq 23 is given by

$$\frac{1}{T_2} = \frac{1}{T_{20}} + \frac{1}{T_{2\text{inter}}} \tag{27}$$

where T_{20} refers to the diamagnetic solution and $T_{2\text{inter}}$ results from the dipolar interaction between the solvent molecule and the free radical. $1/T_{2\text{inter}}$ is proportional to the radical concentration. For the longitudinal relaxation time T_1 we have a relation similar to eq 27. At very low fields, we are in the extreme narrowing case ($\omega_I\tau \ll 1$ and $\omega_S\tau \ll 1$), and it is well known that $T_{1\text{inter}} = T_{2\text{inter}}$ and that the hyperfine splitting A of the radical

TABLE 4: Comparison between the Theoretical and Experimental Values of *r* for Various Temperatures

	$T = 298$ K		$T = 345$ K		$T = 398$ K	
solution	Ib	II	Ib	II	Ib	II
η (SI)	1.9×10^{-3}	9.4×10^{-4}	9.5×10^{-4}	4.4×10^{-4}	5.3×10^{-4}	2.3×10^{-4}
$10^{10} \times D_I$ ($m^2\ s^{-1}$)	5.8[a]	30.35	12[a]	66.6	25.4[a]	147
$10^{10} \times D_S$ ($m^2\ s^{-1}$)	5.7	12.4	11.8	27	25	60
$10^{10} \times D$ ($m^2\ s^{-1}$)[b]	11.5	43	24	94	50	207
$10^{20} \times Db$ ($m^3\ s^{-1}$)	84	202	174	453	273	1001
r (theoretical)	0.21		0.19		0.18	
T_1 (s)[a]	0.6	1.48	0.92	3.8	2.11	7.9
T_{10} (s)[a]	1.8	2.8	5.8	8.75	7.68	18
$1/T_{1inter}$	1.26	0.32	0.86	0.15	0.34	0.07
r (experimental)	0.25		0.17		0.20	

[a] Measured values. [b] $D = D_I + D_S$.

molecule has no effect.[23] For $S = {}^1/_2$ we have

$$\frac{1}{T_{1inter}} = \frac{1}{T_{2inter}} = \left(\frac{\mu_0}{4\pi}\right)^2 \gamma_I^2 \gamma_S^2 h^2 J(0) \tag{28}$$

where $J(0)$ is given[30] by eq 11.

Note that for higher fields such that $0 < \omega_S < A$ with a value of $J(\omega_S\tau)$ which cannot be replaced by $J(0)$, a significant departure from eq 28 is expected. This case will be the object of a separate study. Comparing both solutions Ib and II, we have from eqs 11 and 27

$$r = \frac{T_{1inter}(\mathrm{Ib})}{T_{1inter}(\mathrm{II})} = \frac{1}{2}\frac{Db(\mathrm{Ib})}{Db(\mathrm{II})} \tag{29}$$

In eq 29 the factor 2 arises from the different concentrations of both solutions: 2×10^{-3} mol L^{-1} for solution Ib and 10^{-3} mol L^{-1} for solution II. The corresponding value for this ratio using estimated values of the relative diffusion constant D and of the minimum distances of approach b are provided in Table 4 and is compared with the ratio of the measured values of $1/T_{1inter} = 1/T_1 - 1/T_{10}$. Good agreement is obtained over the whole investigated temperature range. Consequently the lower value of T_2 for solution Ib compared to solution II arises from three effects: a higher concentration and a much lower relative diffusion constant D, essentially due to higher viscosity of triglyme giving shorter values of T_{2inter}, and slightly shorter measured values of T_{20} (2.0 and 2.8 s at $T = 298$ K respectively). On the other hand, the larger size of solvent molecules of solution Ib is a relatively weak unfavorable effect.

Conclusion

We have shown that solution Ib (2×10^{-3} mol L^{-1} of TMIO in triglyme) which is chemically stable in a broad temperature range displays a DNP enhancement factor varying between 1000 and 2000 between 25 and 125 °C. This remarkable result was interpreted with accuracy using the high-field EPR line widths measurements with the help of the relaxation matrix formalism. It was shown that the main contributions to the electronic relaxation arises from the exchange interaction between free radicals, from the spin rotational effect, and from the unresolved hyperfine structure with the protons of the radical molecule. The enhanced NMR signal was shown to have better efficiency in the presence of external magnetic field gradients than the other solutions. This was explained by a shorter nuclear transverse relaxation times of the solvent protons. The solution Ib will be used in the next generation of DNP-NMR magnetometers for oil-prospecting purposes.

Appendix. Calculation of the Dynamic Polarization Factor *F*

(A) Analytical expression for *F*. We summarize and adapt to our solutions a model that allows us to calculate F for solutions containing nitroxide free radicals in low magnetic fields.[27,36] We start from the level scheme of Figure 1 for the free radical, denoting by E_i and $|i\rangle$ the four energy levels and the corresponding eigenstates of the spin Hamiltonian $\mathbf{H}/\hbar = A\vec{S}\cdot\vec{K} + \omega_s S_z$. Let N be the number of free radicals in the sample and $p_i = N_i/N$ the relative populations of these levels. In dynamic equilibrium we have

$$p_i \approx \frac{1}{4}(1 - \beta E_i + x_i) \quad (\beta = 1/kT) \tag{A1}$$

where $\beta E_i \ll 1$ and $x_i \ll 1$. Choosing the origin of the energies such that $\sum E_i = 0$, we have

$$\sum_i x_i = 0 \tag{A2}$$

with $x_i = 0$ at thermal equilibrium. The x_i are considered as the components $\langle i|x\rangle$ of a vector $|x\rangle$ in the four-dimensional space spanned by the states $|i\rangle$. According to eqs 5 and A1, for purely dipolar coupling between the solvent nuclei and the free radical

$$F = -\frac{f}{8I_0}\sum_i \langle i|S_z|i\rangle x_i \tag{A3}$$

Introducing a vector $|v\rangle$ in the same space, such that $\langle i|v\rangle = \langle i|S_z|i\rangle$, we have

$$\sum_i \langle i|S_z|i\rangle x_i = \sum_i \langle v|i\rangle\langle i|x\rangle = \langle v|x\rangle \tag{A4}$$

and F can be rewritten as

$$F = -\frac{f}{8I_0}\langle v|x\rangle \tag{A5}$$

From Figure 1 it is seen that the four components of $|v\rangle$ are $({}^1/_2, \epsilon/2, {}^{-1}/_2, -\epsilon/2)$ We write the time evolution of the four level populations due to the radiofrequency field and represented by transition probabilities of the various relaxation processes. For intramolecular and intermolecular relaxation mechanisms we introduce transition probabilities defined by

$$W_{ij} = \frac{1}{2}(W_{i\to j} + W_{j\to i})$$

$$W_{ik,jl} = \frac{1}{2}(W_{ik\to jl} + W_{jl\to ik}) \tag{A6}$$

with

$$W_{j\to i} = W_{i\to j}\exp[\beta(E_j - E_i)]$$

$$W_{jl\to ik} = W_{ik\to jl}\exp[\beta(E_j + E_l - E_i - E_k)] \tag{A7}$$

After linearization of eq A7 and using eqs A1−A6, the population rate equation is

$$\frac{dN_i}{dt} = -\sum_j [W_{i\to j} + W^{exc}_{i\to j}]N_i + \sum_j [W_{j\to i} + W^{exc}_{j\to i}]N_j - \sum_{j,k,l} W_{ik\to jl}N_iN_k + \sum_{j,k,l} W_{jl\to ik}N_jN_l \quad (A8)$$

where $W^{exc}_{i\to j}$ is the transition rate induced by the external radiofrequency field H_1. Equation A8 can be rewritten as

$$\frac{dx_i}{dt} = \sum_j [(W_{ij} + W^{exc}_{ij})(x_j - x_i) + \beta(E_i - E_j)W^{exc}_{ij}] + \frac{N}{4}\sum_{j,k,l}(W_{ik,jl} + W_{ik,lj} - W_{ij,kl})(x_j - x_i) \quad (A9)$$

In the absence of the external radiofrequency field H_1, eq A9 can be written

$$\frac{d|x\rangle}{dt} = -\mathbf{R}|x\rangle \quad (A10)$$

where we have defined a relaxation matrix **R** in which all the relaxation mechanisms are involved. The matrix elements of **R** are

$$R_{ij} = -W_{ij} - \frac{N}{4}\sum_{k,l}(W_{ik,jl} + W_{ik,lj} - W_{ij,kl}) \quad (i \neq j)$$

$$R_{ii} = -\sum_{j\neq i} R_{ij} \quad (A11)$$

In a state of dynamic equilibrium, we have from eqs A9 and A11

$$\sum_j R_{ij}x_j + \sum_j W^{exc}_{ij}(x_i - x_j) = \beta\sum_j (E_i - E_j)W^{exc}_{ij} \quad (A12)$$

If the rf field only involves the $1 \leftrightarrow 4$ transition, we define a vector $|\alpha_1\rangle = |1\rangle - |4\rangle$ and eq A12 becomes

$$(\mathbf{R} + W^{exc}|\alpha_1\rangle\langle\alpha_1|)|x\rangle = \beta(E_1 - E_4)W^{exc}|\alpha_1\rangle = \beta\hbar\omega_{14}W^{exc}|\alpha_1\rangle \quad (A13)$$

The linear system A13 is singular because the vector $|u_1\rangle$ with all components $\langle i|u_1\rangle = 1$ is an eigenstate of the left-hand side of eq A13 for the zero eigenvalue. It is easy to remove this singularity by adding to the matrix **R** the matrix $\lambda|u_1\rangle\langle u_1|$ ($\lambda \neq 0$) which does not affect the system A10 because according to eq A2 $\langle u_1|x\rangle = \sum_i x_i = 0$. Then defining

$$\mathbf{R}' = \mathbf{R} + k|u_1\rangle\langle u_1| \quad (A14)$$

where $\mathbf{R}'$ is a symmetrical regular matrix, the linear form $\langle v|x\rangle$, defined by eq A4, becomes

$$\langle v|x\rangle = \beta\hbar\omega_{14}W^{exc}\langle v|[\mathbf{R}' + W^{exc}|\alpha_1\rangle\langle\alpha_1|]^{-1}|\alpha_1\rangle = \beta\hbar\omega_{14}W^{exc}\sum_{n=0}^{\infty}(-W^{exc})^n\langle v|(\mathbf{R}'^{-1}|\alpha_1\rangle\langle\alpha_1|)^n\mathbf{R}'^{-1}|\alpha_1\rangle = \beta\hbar\omega_{14}W^{exc}\sum_{n=0}^{\infty}(-W^{exc})^n\langle v|\mathbf{R}'^{-1}|\alpha_1\rangle\langle\alpha_1|\mathbf{R}'^{-1}|\alpha_1\rangle^n$$

Finally we have

$$\langle v|x\rangle = \beta\hbar\omega_{14}W^{exc}\frac{\langle v|\mathbf{R}'^{-1}|\alpha_1\rangle}{1 + W^{exc}\langle\alpha_1|\mathbf{R}'^{-1}|\alpha_1\rangle} \quad (A15)$$

Depending on the presence of two electronic transitions ω_{14} and ω_{34}, separated by only $\Delta\omega = \omega_S$, it is impossible to select one of these transitions with an rf field. If W^{exc} is the transition probability for the $1 \leftrightarrow 4$ transition, we denote by kW^{exc} the corresponding value for the $3 \leftrightarrow 4$ transition. Introducing the vector $|\alpha_2\rangle = |3\rangle - |4\rangle$, eq A13 becomes

$$[\mathbf{R}' + W^{exc}|\alpha_1\rangle\langle\alpha_1| + kW^{exc}|\alpha_2\rangle\langle\alpha_2|]|x\rangle = \beta W^{exc}\hbar(\omega_{14}|\alpha_1\rangle + k\omega_{34}|\alpha_2\rangle) \quad (A16)$$

In order to solve this system where, as above, we have replaced the singular matrix **R** by $\mathbf{R}'$ defined by eq A14, we seek a solution of the form

$$|x\rangle = \beta\hbar\mathbf{R}'^{-1}(y_1\omega_{14}|\alpha_1\rangle + y_2\omega_{34}|\alpha_2\rangle) = \beta A\hbar\mathbf{R}'^{-1}\left[\left(1 + \frac{\epsilon}{2}\right)y_1\left|\alpha_1\right\rangle + \left(1 - \frac{\epsilon}{2}\right)y_2\left|\alpha_2\right\rangle\right] \quad (A17)$$

with $\epsilon = \omega_S/A$

As $|\alpha_1\rangle$ and $|\alpha_2\rangle$ are independent vectors, using eq A17, we obtain the following system equivalent to eq A16

$$\left(\frac{1}{W^{exc}} + R_{11}\right)y_1 + \frac{\omega_{34}}{\omega_{14}}R_{12}\,y_2 = 1$$

$$\frac{\omega_{14}}{\omega_{34}}R_{21}y_1 + \left(\frac{1}{kW^{exc}} + R_{22}\right)y_2 = 1 \quad (A18)$$

with $\omega_{34}/\omega_{14} \approx 1 + \epsilon$, and $R_{ij} = \langle\alpha_i|\mathbf{R}'^{-1}|\alpha_j\rangle$. The solutions of eq A18 are

$$y_1 = W^{exc}\frac{1 + kW^{exc}[R_{22} - (1-\epsilon)R_{12}]}{1 + W^{exc}[R_{11} + R_{22}] + k(W^{exc})^2\Delta a}$$

$$y_2 = kW^{exc}\frac{1 + W^{exc}[R_{11} - (1+\epsilon)R_{21}]}{1 + W^{exc}[R_{11} + kR_{22}] + k(W^{exc})^2\Delta a} \quad (A19)$$

with $\Delta a = R_{11}R_{22} - R_{12}R_{21}$.

Finally, from eq A17, the dynamic polarization factor given by eq A5, where $I_0 = \beta\hbar\omega_I/4$, becomes

$$F = -\frac{A}{2\omega_I}f\left\langle v\left|\mathbf{R}'^{-1}\left[\left(1 + \frac{\epsilon}{2}\right)y_1\left|\alpha_1\right\rangle + \left(1 - \frac{\epsilon}{2}\right)y_2\left|\alpha_2\right\rangle\right]\right\rangle = -\frac{A}{2\omega_I}f\Phi \quad (A20)$$

which defines the function Φ introduced in eq 6.

In order to determine F, we need the relaxation matrix elements and the expressions for W^{exc} and k.

Assuming independent Lorentzian line shapes, with a radio frequency excitation field $H_1 \cos \omega t$ along the x direction, we have

$$W^{exc} = \frac{(\gamma_S H_1)^2}{2}\langle 1|S_x|4\rangle^2\frac{(T_2)_{14}}{1 + (T_2)^2_{14}(\omega - \omega_{14})^2} \quad (A21)$$

where $(T_2)_{14}$ is the transverse weak field relaxation time for the transition $|1\rangle \leftrightarrow |4\rangle$ and $\langle 1|S_x|4\rangle^2 = {}^1/_8\,(1 + \epsilon)$. Consequently,

with obvious notations, we have

$$k = \frac{W_{34}}{W_{14}} = \frac{|\langle 3|S_x|4\rangle|^2}{|\langle 1|S_x|4\rangle|^2}\frac{(T_2)_{34}}{(T_2)_{14}}\frac{1+(T_2)_{14}^2(\omega-\omega_{14})^2}{1+(T_2)_{34}^2(\omega-\omega_{34})^2} \quad \text{(A22)}$$

(B) Elements of the Relaxation Matrix R. The detailed theory giving the relaxation matrix **R** has been given elsewhere.[14] Each of the four relaxation processes given in section II taken separately leads to a relaxation matrix. It is assumed that **R** is obtained by addition of the various contributions. We use the extreme narrowing approximation, which is justified by the fact that in the investigated temperature range the solutions have a rather low viscosity, leading to the condition $\omega_{ij}\tau \ll 1$, where τ are the various correlation times. It is then possible to relate the contribution of each relaxation process to its contribution to the transverse relaxation rate $(1/T_2)^X$ in the X band (9 GHz) which is itself related through eq 7 to the line width contribution ΔH^X. One has

for the spin rotational interaction

$$R_{ij}^{SR} = \left(\frac{1}{T_2}\right)_{SR}^{X}\left[\frac{3}{4}\delta_{ij} - \left|\langle j|\vec{S}|i\rangle\right|^2\right] \quad \text{(A23)}$$

for the magnetic dipolar coupling between free radicals

$$R_{ij}^{DIP} = \frac{60}{19}\left(\frac{1}{T_2}\right)_{DIP}^{X}\left[\frac{3}{4}\delta_{ij} + \frac{1}{2}\langle i|S_z|i\rangle\langle j|S_z|j\rangle - \left|\langle i|\vec{S}|j\rangle\right|^2\right] \quad \text{(A24)}$$

for the exchange coupling between free radicals

$$R_{ij}^{EX} = \frac{3}{2}\left(\frac{1}{T_2}\right)_{EX}^{X}\left[\frac{3}{4}\delta_{ij} - \left|\langle i|\vec{S}|j\rangle\right|^2 - 2\langle i|S_z|i\rangle\langle j|S_z|j\rangle\right] \quad \text{(A25)}$$

Concerning the modulation of the hyperfine field, it is not useful to relate R_{ij}^{HF} to $(1/T_2)_{HF}^{X}$, as this contribution to the EPR line width in the X band cannot be separated from the modulation of the Lande Factor. The latter effect becomes negligible in Earth's magnetic field, and, for that reason, we directly express, R_{ij}^{HF} with $(1/T_2)_{HF}$ in low fields. We have

$$R_{ij}^{HF} = -\frac{24}{5}\left(\frac{1}{T_2}\right)_{HF}\sum_{\mu=-2}^{\mu=2}|\langle j|T_\mu|i\rangle|^2 \quad \text{(A26)}$$

where the T_μ are the usual second-order spherical tensor components for dipolar coupling between $\vec{S}$ and $\vec{K}$ vectors.[25] Defining

$$a = \frac{1}{4}\left(\frac{1}{T_2}\right)_{SR}^{X};\quad b = \frac{3}{5}\left(\frac{1}{T_2}\right)_{HF};\quad c = \frac{15}{38}\left(\frac{1}{T_2}\right)_{DIP}^{X};\quad d = \frac{3}{8}\left(\frac{1}{T_2}\right)_{EX}^{X} \quad \text{(A27)}$$

and using eqs A23−A26 it is easy to obtain the matrix elements R_{ij}. As explained above the resulting relaxation matrix is singular and is replaced by $\mathbf{R'} = \mathbf{R} + \lambda|u_1\rangle\langle u_1|$. Choosing $\lambda = a + 2c + d$, which is equivalent to adding the same constant λ to all the elements of **R**, the following symmetric $\mathbf{R'}$ matrix is derived

$$\mathbf{R'} = \begin{bmatrix} 3a+3b+7c+2d & -b+(a+3c)\epsilon & a-2b+c+2d & -(a+3c)\epsilon \\ -b+(a+3c)\epsilon & 4a+2b+8c+4d & -b-(a+3c)\epsilon & 0 \\ a-2b+c+2d & -b-(a+3c)\epsilon & 3a+3b+7c+2d & (a+3c)\epsilon \\ -(a+3c)\epsilon & 0 & (a+3c)\epsilon & 4a+8c+4d \end{bmatrix} \quad \text{(A28)}$$

Finally in eq A21, the transverse relaxation time $(T_2)_{14}$ in low fields (Earth's magnetic field) is involved. It has been established[14,15,27,28] that the various contributions of the relaxation processes to $1/T_2$ are related to those of $(1/T_2)^X$ by

$$\left(\frac{1}{T_2}\right)_{SR} = \frac{3}{4}\left(\frac{1}{T_2}\right)_{SR}^{X},\quad \left(\frac{1}{T_2}\right)_{DIP} = \frac{45}{19}\left(\frac{1}{T_2}\right)_{DIP}^{X},\quad \left(\frac{1}{T_2}\right)_{EX} = \frac{3}{4}\left(\frac{1}{T_2}\right)_{EX}^{X} \quad \text{(A29)}$$

Then according to eqs A27 and A29

$$\frac{1}{(T_2)_{14}} = 3a + \frac{5}{3}b + 6c + 2d \quad \text{(A30)}$$

Consequently the function Φ appearing in the expression 6 or A20 of F can be expressed in terms of the four constants defined by eq A27.

References and Notes

(1) Abragam, A. *Phys. Rev.* **1955**, *98*, 1729.
(2) Warmuth-Müller, W.; Meise-Gresch, K. *Adv. Magn. Reson.* **1983**, *1*, 11.
(3) Abragam, A.; Combrisson, J.; Solomon, I. *C. R. Acad. Sci.* **1957**, 157.
(4) Solomon, I. *J. Phys. Radium* **1958**, *19*, 837.
(5) Landesman A. *J. Phys. Radium* **1959**, *20*, 937.
(6) Besson, R.; Lemaire, H.; Rassat, A.; Servoz Gavin, P. *Proceedings of the XIIth Colloque Ampère, Bordeaux 1963*; Servant, R., Charru, A., Eds.; North-Holland: Amsterdam, 1964, p 327.
(7) Lebedev, L. O.; Knidekel, M. L. *Dokl Akad. Nauk SSSR* **1961**, *140*, 1327.
(8) Chiarelli, R.; Rassat, A. *Tetrahedron* **1973**, *29*, 3639.
(9) Rozantzev, E. G.; Mamedova, Y. G.; Neiman, M. B. *Izv. Akad. Nauk SSSR* **1962**, 2250.
(10) Besson, R. Thesis, Université de Grenoble, 1973.
(11) Glazer, R. L.; Poindexter, E. H. *J. Chem. Phys.* **1971**, *55* (9), 4548.
(12) Poindexter, E. H.; Stewart, J. R.; Caplan, J. P. *J. Chem. Phys.* **1968**, *47* (8), 2862.
(13) Ayant, Y.; Besson, R.; Salvi, A. *J. Phys.* **1975**, *36*, 571.
(14) Ayant, Y.; Besson, R.; Casalegno, R. *J. Phys.* **1980**, *41*, 1183.
(15) (a) Sechehaye, R. Thesis, Université de Genève, 1974. (b) Sechehaye, R.; Borcard, B.; Hiltbrand, E.; Béné, G. *Helv. Phys. Acta* **1972**, *45*, 845.
(16) Ferroud-Plattet, M. P.; Berchadsky, Y.; Belorizky, E.; Tordo P. *Ber. Bunsen-Ges Phys. Chem.* **1992**, *96*, 12.
(17) Ferroud-Plattet, M. P.; Ayant, Y.; Belorizky, E.; Tordo, P. *Solid State Commun.* **1991**, *80*, *11*, 947.
(18) Culcasi, M.; Berchadsky, Y.; Gronchi, G.; Tordo, P. *J. Org. Chem.* **1991**, *56*, 3537.
(19) Kernevez, N.; Glénat, H. *IEEE Trans. Magn.* **1991**, *27*, 6.
(20) Kernevez, N.; Duret, D.; Moussavi, M.; Léger, J. M. *IEEE Trans. Magn.* **1992**, *28*, 5.
(21) Bolton, R.; Gillies, D. G.; Sutcliffe, L. H.; Wu, X. *J. Chem. Soc., Perkin Trans. 2* **1993**, *11*, 2049.
(22) Pozzi, J. P.; Barthès, V.; Thibal, J.; Pocachard, J.; Lim, M.; Thomas, T.; Pagès, G. *J. Geophys. Res.* **1993**, *98*, B5, 7939.
(23) Abragam, A. *The principles of nuclear magnetism*; Clarendon Press: Oxford, 1961, Chapter VIII.
(24) Hubbard, P. S. *Proc. R. Soc. London* **1966**, *A291*, 537.
(25) Wilson, R.; Kivelson, D. J. *J. Chem. Phys.* **1966**, *44*, 154.
(26) Ayant, Y. *J. Phys.* **1976**, *37*, 219.
(27) Ayant, Y.; Casalegno, R. *J. Phys.* **1978**, *39*, 325.
(28) Atkins, P. W.; Kivelson, D. J. *J. Chem. Phys.* **1966**, *44*, 169.
(29) Belorizky, E.; Fries, P. H.; Gorecki, W.; Jeannin, M.; Roby, C. *J. Phys. Chem.* **1994**, 98.
(30) Ayant, Y.; Belorizky, E.; Gallice, J. *J. Phys.* **1975**, *36*, 991.
(31) Salvi, C. *Mémoire DPE* 1989, Chapter II.
(32) Van der Drift, E.; Rousseuw, B. A. C.; Smidt, J. *J. Phys.* **1984**, *88*, 2275.
(33) Ferroud-Plattet, M. P. Thesis, Université de Grenoble, 1992.
(34) Abragam, A.; Bleaney, B. *RPE des ions de transition*; PUF: Paris, 1971.
(35) (a) Connoly, M. L. *Science* **1983**, *221*, 709. (b) Connoly, M. L. *J. Appl. Crystallogr.* **1983**, *16*, 548.
(36) Casalegno, R. Thesis, Université de Grenoble, 1978.